J Fluoresc (2008) 18:253–259
DOI 10.1007/s10895-007-0242-9

ORIGINAL PAPER

Study of Structural and Photoluminescent Properties of $Ca_8Eu_2(PO_4)_6O_2$

C. C. Silva · F. P. Filho · A. S. B. Sombra · I. L. V. Rosa · E. R. Leite · E. Longo · J. A. Varela

Received: 12 December 2006 / Accepted: 14 August 2007 / Published online: 1 December 2007

Abstract In this work it is presented for the first time the nanostructured hydroxyapatites doped with 0.5, 1.0 and 2.0 wt% of Eu^{3+} prepared at room temperature by the mechanical alloying technique. X-ray diffraction powder (XRD), infrared (IR) and Raman scattering spectroscopy, scanning electron microscopy (SEM), microhardness measurements as well as luminescent data of Eu^{3+} were used to investigate the structural and optical properties of these nanomaterials. The electrical and dielectrical analyses were used with the intention of having a better comprehension about the electromagnetic fields in pure and doped hydroxyapatites.

C. C. Silva · F. P. Filho
Metallurgical and Materials Engineering Department,
Federal University of Ceará Campus do Pici,
714 Block,
60455-760 Fortaleza, Ceará, Brazil

C. C. Silva
e-mail: ccsilva@fisica.ufc.br

C. C. Silva · A. S. B. Sombra
Telecommunications and Materials Science and Engineering
Laboratory (LOCEM), Physics Department,
Federal University of Ceará, Campus do Pici,
6030, 60455-760 Fortaleza, Ceará, Brazil

I. L. V. Rosa (✉) · E. R. Leite
Laboratório Interdisciplinar de Eletroquímica e Cerâmica,
CMDMC, Departamento de Química,
Universidade Federal de São Carlos,
Via Washington Luiz, Km 235,
CEP:13565-905 São Carlos, SP, Brazil
e-mail: ilvrosa@power.ufscar.br

E. Longo · J. A. Varela
CMDMC, LIEC, Instituto de Química,
Universidade Estadual Paulista,
CEP: 14801-907 Araraquara, SP, Brazil

Keywords Hydroxyapatite · Nanomaterial · Europium · Photoluminescence

Introduction

Apatite family has the general formula $M_{10}(XO_4)_6Y_2$ (M = Ca^{2+}, Sr^{2+}, Ba^{2+}; XO_4 = PO_4^{3-}, VO_4^{3-}, AsO_4^{3-} and Y = OH^-, F^-, Cl^-) which belongs to the $P6_3/m$ space group. Hydroxyapatite, $Ca_{10}(PO_4)_6(OH)_2$, is mainly used in reconstructive orthopedics and dental surgery playing the role of massive filling of bone gaps and coating the bone surface promoting adhesion between prostheses and bone [9, 10]. Lots of papers deal with the study of hydroxyapatite as a substitute for the human bone [11–16]. The substitution of M^{2+}cation for rare earth ions in this material prepared by the solid state reaction at high temperature has been extensively studied [1–8]. Mechanochemical syntheses of $Ca_{10}(PO_4)_6(OH)_2$ were already studied before, where the materials have to be heated at 1250°C [17] and 1100°C [18] to have the $Ca_{10}(PO_4)_6(OH)_2$ single phase, but these methods did was not a completely dry ones. The mechanical alloying was successfully used to produce nanocrystalline powders of hydroxyapatite using different experimental procedures [19, 20]. The structural and electrical properties of the biosystem with calcium and sodium phosphate obtained for microwave irradiation were also studied [21].

The luminescent properties of rare earth compounds have been widely used since they can be employed as visible, near-IR radiation sources, besides their use as laser and optical communication devices, especially when they dope phosphate compounds as apatites [22–24]. Trivalent europium (Eu^{3+}) has been also used as a tool to probe the local symmetry and occupancy at the cationic sites in the structure of oxyapatites and fluorapatites [25–30]. Recently

an Eu^{3+} doped calcium-deficient apatite, $Ca_9(PO_4)_5(HPO_4)(OH)$, synthesized in hydroalcoholic medium was obtained where Eu^{3+} ion was proposed as a biological probe [31]. The study of the electrical and dielectrical properties of $Ca_{10}(PO_4)_6(OH)_2$ (HAP) is an important scientific issue since electromagnetic fields have been shown to accelerate healing in bone fractures, and has created technological interest due to the promising application of this material as biological sensors [32].

In this work nanostructured hydroxyapatites (HAP) doped with 0.5, 1.0 and 2.0 wt% of Eu^{3+}, denoted as HAP:Eu0.5, HAP:Eu1.0, and HAPEu:2.0 were prepared at room temperature by mechanical alloying technique for the first time. X-ray diffraction powder (XRD), infrared (IR) and Raman scattering spectroscopy, scanning electron microscopy (SEM) as well as luminescent properties of Eu^{3+} were used to investigate the structural and optical properties of these nanomaterials. Electrical and dielectrical properties of these powders were used with the intention of having a better comprehension about the electromagnetic fields in these samples.

Experimental procedure

The milling powder procedure

The $Ca_{10}(PO_4)_6(OH)_2$ powder, HAP, was prepared by mechanical alloying using the following experimental procedure.

$$7Ca(OH)_2 + 3Ca(H_2PO_4)_2 \xrightarrow{IMPACTS} Ca_{10}(PO_4)_6(OH)_2 + 12H_2O$$

The commercial reagents $Ca(H_2PO_4)_2$ (Aldrich, 85%), $Ca(OH)_2$ (Vetec, 97% with 3% of $CaCO_3$) and Eu_2O_3 (Aldrich, 99,99%) were used without previous purifications. In this experimental procedure, the appropriate amount of the start materials was ground on a Fritsch Pulverisette 6 planetary mill with the stoichiometric proportionality between then as given up by the above chemical equation. Milling was performed in sealed stainless steel vials balls in air, with 370 rpm as rotation speed. The ratio between powders to the ball mass used in all the procedures was near 1/6. The milling was performed in 60 min milling steps with 10 min pauses to avoid excessive heating. Mechanical alloying was performed for 20 hours of milling. The pure hydroxyapatite (HAP) was doped with 0.5; 1.0 and 2.0 wt% of europium, resulting HAP:Eu0.5, HAP:Eu1.0, and HAPEu:2.0 samples. The Eu_2O_3 used for doping the powders was previously calcinated at 1150°C for 24 hours with heating rate of 4°C/min. The samples HAP:Eu0.5, HAP:Eu1.0, and HAP:Eu2.0 were obtained and characterized by X-ray diffraction powder (XRD), infrared (IR) and Raman scattering spectroscopy, scanning electron microscopy (SEM) as well as through the luminescent properties of Eu^{3+}. These techniques were used to investigate the structural and optical properties of these materials. Besides, the analysis of the electrical and dielectrical properties of $Ca_{10}(PO_4)_6(OH)_2$ were also studied.

X ray diffraction

The X-ray diffraction (XRD) patterns were obtained at room temperature, using powdered and bulk samples, in a PHILIPS X'PERT system, with a K_α radiation (Cu_λ= 1.54056 Å) at 40 kV and 30 mA, with a step of 0.02 and a time per step of 1 s using the geometry of Bragg-Brentano.

Dielectric measurements

The Dielectric measurements were obtained from a HP 4291A Material Impedance Analyzer in conjunction with a HP 4194 Impedance Analyzer, which jointly cover the region of 100 Hz to 1.8 GHz at room temperature (300 K). For the electrical measurements the disc shaped samples, with 5×10^{-3} m of diameter and approximately 1 mm of thickness, were mechanically compressed between two parallel stainless steel electrodes.

Micro hardness vickers

Micro hardness measurements were made by measuring Vickers indentations on the no polished faces of the doped hydroxyapatite with europium specimens using a Vickers Micro Hardness Test (HMV-2 SHIMADZU). Load of 9.81 N were used with a 20 s loading time and loading speed of 70 μm/s, and were made approximately 10 to 20 indentations per specimens. The Vickers Hardness (H_V) of the sintered hydroxyapatite samples was calculated using the average diagonal length of the Vickers indentation as depicted in equation 1:

$$H_V = \frac{l}{2d^2} \quad (1)$$

Where l is the indentation load in Newton (N) and $2d$ is the length of the indentation diagonal in meters. All samples were thermally etched by heating the specimens in air in a conventional furnace at 900°C for 5 hours.

Scanning electron microscopy

Microstructure was performed in a HITACHI S4100-1 system, on the surface of all samples covered with carbon before microscopic observation.

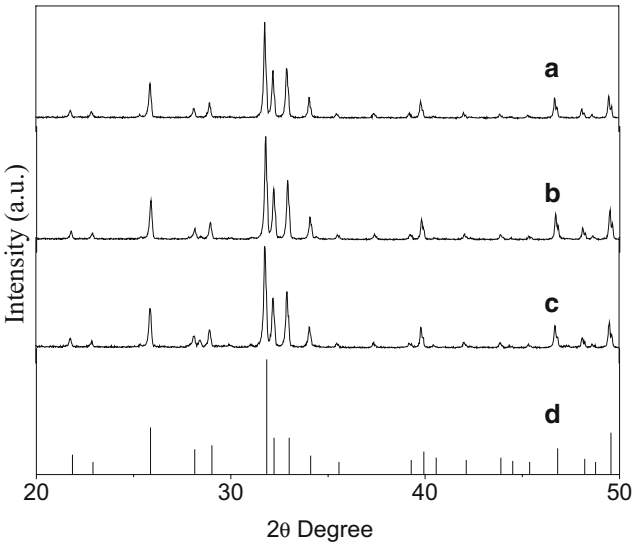

Fig. 1 XRD patterns of the HAP:Eu0.5 (**a**), HAP:Eu1.0 (**b**) and HAP:Eu2.0 (**c**) samples synthesized by the milling reaction. Pecks related to the $Ca_8Eu_2(PO_4)_6O_2$ phase are shown in (**d**) as JCPDS-Pattern 33-0275 [33]

Luminescence measurements

Emission and excitation spectra were obtained under a 450 W xenon lamp in a Jobin Yvon-Fluorolog. Luminescence lifetime measurements were carried out as well using a 1934D model spectrophosphorometer coupled to the spectrofluorometer.

Results and discussion

Figure 1 presents the XRD patterns for hydroxyapatites HAP:Eu0.5 (a), HAP:Eu1.0 (b) and HAP:Eu2.0 (c). It can be noticed that all samples presented a good phase identification when compared to the JCPDS–Pattern 33-0275 ($Ca_8Eu_2(PO_4)_6O_2$) [33] showed at (d), indicating that the milling reaction resulted in an excellent substitution of the calcium for europium ions.

Table 1 show the microhardness data for HAP, HAP:Eu0.5, HAP:Eu1.0 and HAP:Eu2.0 samples, where it is observed an increase of these values as the amount of europium oxide increase. This behavior characterizes an interference of the europium in the $Ca_8Eu_2(PO_4)_6O_2$ structure as Ca^{2+} is replaced by Eu^{3+} during the milling process. This behavior could be related to the grains morphology of the material. It is a well-established fact that ceramic hardness depends on the grain sizes. Smaller grain sizes yield higher hardness values [34]. As it is observed at Figs. 2, 3 and 4, which show SEM micrograph of the samples HAP:Eu0.5, HAP:Eu1.0 and HAP:Eu2.0, these materials present a different morphology, which reveals an homogeneous aspect of the synthesized particles for all samples. The HAP:Eu0.5 and HAP:Eu2.0 samples show a much more homogeneous morphology of the grains than the HAP:Eu1.0 one, which presents a flat shape at the surface (see Fig. 3).

Table 1 Microhardness Vickers (H_V) in MPa for the HAP, HAP:Eu0.5, HAP:Eu1.0 and HAP:Eu2.0 samples

Samples	Microhardness (MPa)
HAP	278
HAPEu0.5M	510
HAPEu1M	418
HAPEu2M	710

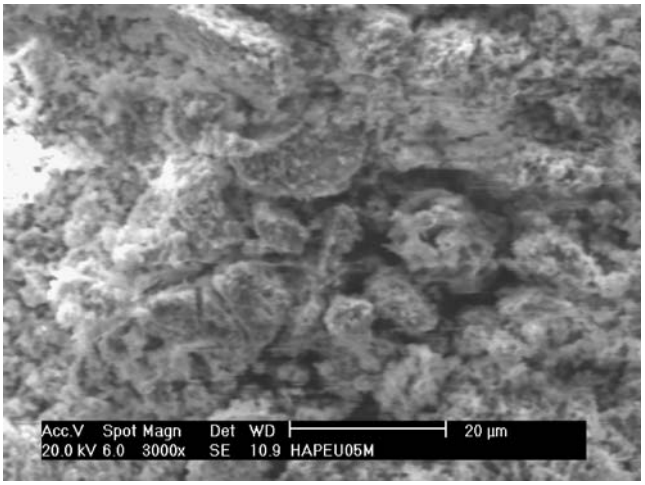

Fig. 2 Scanning electron micrographs of the sample HAP:Eu0.5

Table 2 presents the dependence of dielectric constants data (ε′) for the HAP, HAP:Eu0.5, HAP:Eu1.0 and HAP:Eu2.0 samples in 1 MHz frequency. It is observed a decrease in the å′ values as the Eu^{3+} is incorporated to HAP, compared to this sample, which presents the value of 11.3 for the ε′. The dielectrical properties are associated with the motions of OH^- ions in the HAP phase [35]. The

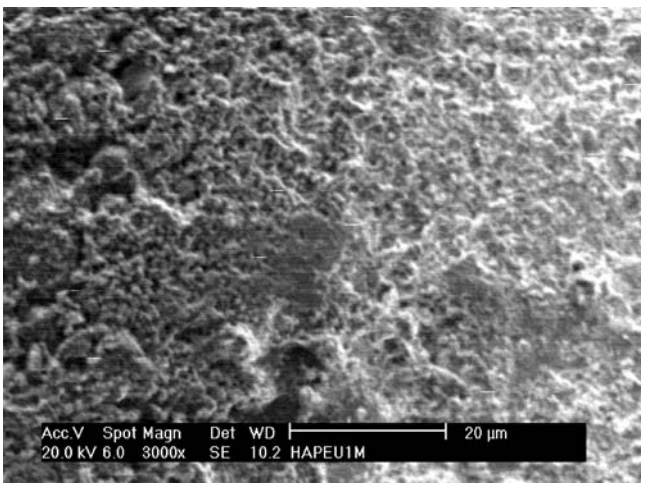

Fig. 3 Scanning electron micrographs of the sample HAP:Eu1.0

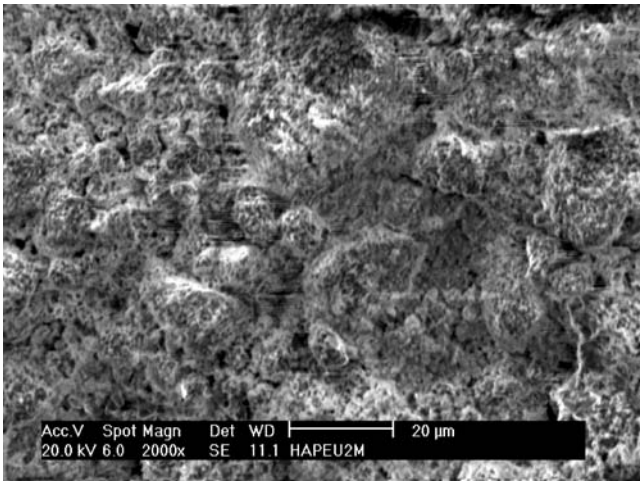

Fig. 4 Scanning electron micrographs of the sample HAP:Eu2.0

incorporation of Eu^{3+} in the HAP leads to the formation of the $Ca_8Eu_2(PO_4)_6O_2$ phase, causing a decrease of the electrical dipoles of OH^- ions, promoting the decrease of the ε′ values. These results show that Eu^{3+} concentration is a very important factor for the dielectrical properties of these materials, and it is related to the substitution of OH^- for Eu^{3+} ions.

The particularities of the luminescence of rare earth like long decay time and narrow-band emission spectra are responsible for the high importance of these ions. The lanthanide spectroscopic properties are due to the fact that in its ions the excited and ground states possess the 4f electronic configuration whose 4f electrons are shielded by the outer **s** and **p** electrons protecting them from the external surrounding. Eu^{3+} has a spectrum easily comprehensible due to its simplicity, so it has been the most studied by luminescence spectroscopy among the rare earth ions. The luminescence spectrum of the Eu^{3+} presents a relatively simple energy level structure with the emission lines extending from visible to near infrared region. Especially the $^5D_0 \rightarrow {}^7F_J$ (J=0,1,2,...6) manifold capacitates one to determine the microscopic symmetry around the site, making the Eu^{3+} an ideal experimental probe of the crystalline environment [36]. The Eu^{3+} ion normally excited by 394 nm light, correspondent to the $^5L_6$ level, decays in inorganic systems to the ^5D levels, mainly to the $^5D_0$ one, from which the ground state is reached with emission of radiation to the levels of the fundamental term ^7F_J

Table 2 Dielectric constants (ε′) data for the HAP, HAP:Eu0.5, HAP:Eu1.0 and HAP:Eu2.0

Samples	ε′
HAP	11.3
HAPEu0.5M	6.7
HAPEu1M	6.5
HAPEu2M	6.8

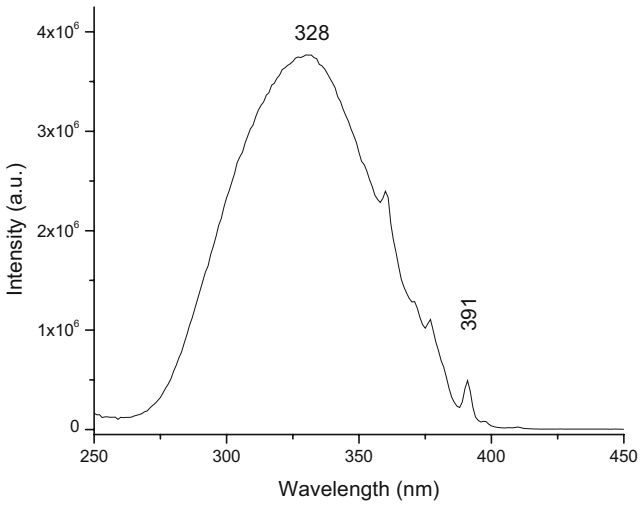

Fig. 5 Excitation spectra of the HAP:Eu2.0 sample recorded with the emission set at 573 nm at room temperature

(J=0,1,2,... 6) [37]. The crystal field at the location of the free ion may break the (2J+1) degenerescence. The levels with J=0 are normally not degenerated, so the $^5D_0 \rightarrow {}^7F_0$ transition shows no more than one band at the spectrum. The $^5D_0 \rightarrow {}^7F_1$ transition appears at least as three bands, five bands is expected for $^5D_0 \rightarrow {}^7F_2$, seven bands for $^5D_0 \rightarrow {}^7F_3$ and so on. When this behavior is observed it is supposed that Eu^{3+} sites have a unique symmetry. Changes in the surrounding can cause only a slight change in the position

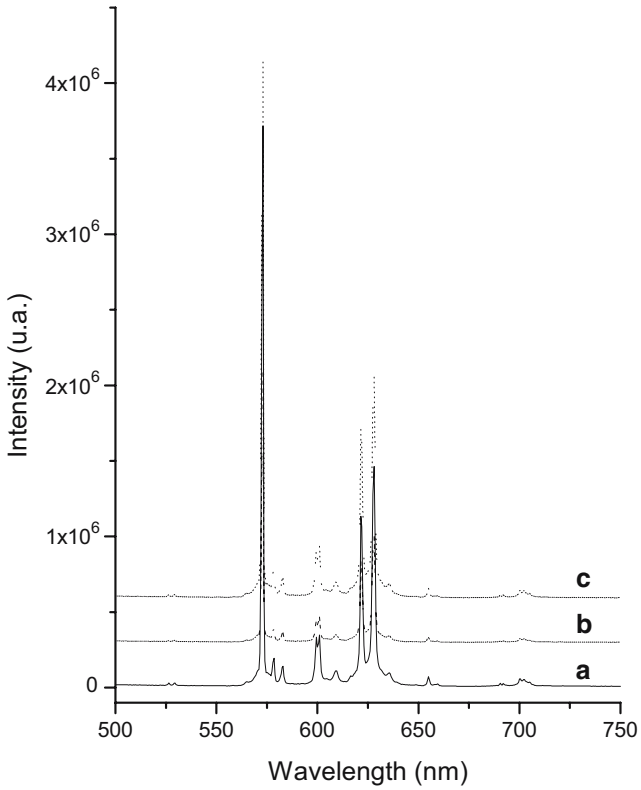

Fig. 6 Emission spectra of the HAP:Eu0.5 (**a**), HAP:Eu1.0 (**b**) and HAP:Eu2.0 (**c**) samples, excited at 328 nm at room temperature

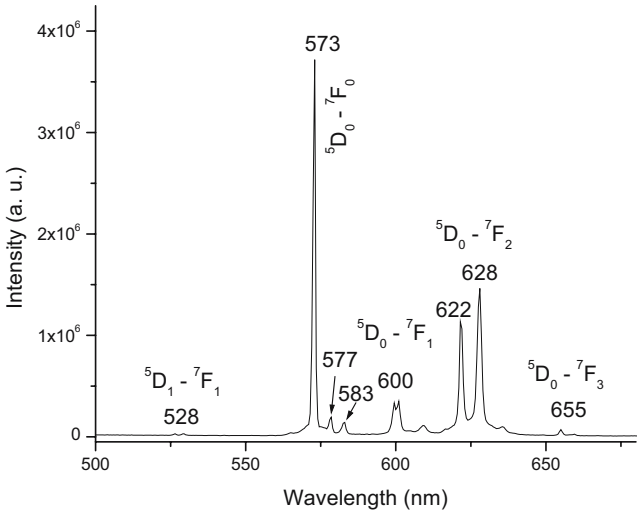

Fig. 7 Emission spectra of the HAP:Eu0.5 sample, excited at 328 nm at room temperature, indicating the Eu^{3+} $^5D_{0,1} \rightarrow {}^7F_J$, J=0, 1, 2, 3 and 4, transitions

of the electronic transition lines of the rare earth ions; very different values in its luminescence lifetime however, have been observed [38, 39].

Figure 5 show excitation spectra of HAPEu2.0 sample recorded with the emission set at 573 nm, the highest emission intensity, at room temperature. As it is observed in this Figure, there is a strong and broad excitation band with a maximum at 328 nm, probably related to the ligand-metal charge transfer into the hydroxyapatite matrix. It is also observed a weak band at 391 nm ascribed to the $^5L_6$ level of the Eu^{3+}, as it is commonly observed in numerous inorganic systems. Unfortunately, rare earth ions absorb very little excitation energy since the f*–f* transitions are forbidden by the Laporte rule. The presence of the strong band at 328 nm indicates an increasing light absorption cross section as it is observed by antenna effect which is present in lanthanide complexes [40, 41]. In the case of doped HAP however, we do not have the disadvantages of the low thermal and mechanical stability observed in the complexes, which limits their further application. In hydroxyapatite matrix the interaction among the inorganic components occurs through the powerful covalent bonds, which build its single phase.

Figure 6 show the emission spectra of the HAP:Eu0.5, HAP:Eu1.0 and HAP:Eu2.0 samples, excited at 328 nm at room temperature. It was not observed a significant change in the spectra behaviour as the Eu^{3+} concentration is increased. It is only observed a slight difference in its intensity. The feature of these Eu^{3+} emission spectra have the same characteristic bands as reported in some literature on luminescence data [42–44].

Figure 7 show the emission spectra of the HAP:Eu0.5 sample, excited at 328 nm at room temperature. The weak bands at around 528 nm are ascribed to the $^5D_1 \rightarrow {}^7F_1$ transition of the Eu^{3+} emission. The Eu^{3+} $^5D_0 \rightarrow {}^7F_0$ transition is observed as the strongest peak at 573 nm. The very weak peak at 577 nm is also attributed to this Eu^{3+} transition, indicating the presence of this ion in the B site [43]. It is difficult to say in this case that the main $^5D_0 \rightarrow {}^7F_0$ transition at 573 nm is non-degenerated, since we did not perform low temperature measurement neither site-selective excitation of a particular site or level, but it is possible to see that there are the A_1 and A_2 nonequivalent crystallographic sites of Eu^{3+} in this material. The emission spectrum of the

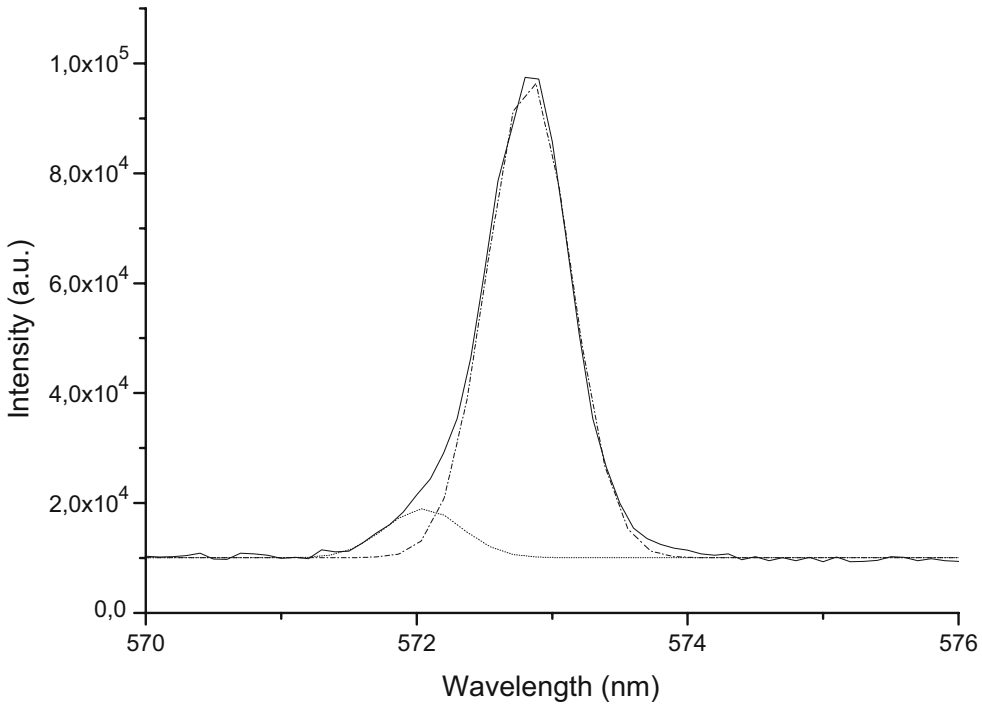

Fig. 8 Emission spectra of the HAP:Eu0.5 sample, excited at 328 nm at room temperature with simulations (*dotted line*)

HAP:Eu0.5 sample, excited at 328 nm at room temperature with simulations (dotted line) at Fig. 8 presents the $^5D_0 \rightarrow {}^7F_0$ transition at 573 nm, where it is noticed a slight shoulder at around 572 nm. The high intensity of the band at 573 nm also indicates that both positions related to A_1 and A_2 correspond to a preponderance site, while the weak band at 577 nm (Fig. 7) suggests to a minority site. The hydroxyapatite (HAP), $Ca_{10}(PO_4)_6(OH)_2$, crystallizes in the hexagonal system, which space group is $P6_3/m$. This structure presents two kinds of cationic sites. The M(I) site has trigonal point symmetry (C_3) corresponding to the 4f site, and it is formed by nine oxygen atoms belonging to the phosphate groups surrounding the cationic site. The M(II) site corresponds to the 6h positioning a sevenfold coordination with six oxygen atoms belonging to phosphate groups and one OH anion, which local symmetry is C_s [44]. According to several literature studies [42–44], Eu^{3+} substitute Ca^{2+} ions and occupy mainly the Ca (II) sites, which a relative abundance of 60%. The intense $^5D_0 \rightarrow {}^7F_0$ emission band at 573 nm (A_1 and A_2 sites) is related to this substitution. While the weak band at 577 nm (B site) is attributed to the substitution on Ca (I) sites, which has a relative abundance of 40%. It is also noticed in Fig. 7 the presence of the $^5D_0 \rightarrow {}^7F_2$ transition with two strong bands at 622 and 629 nm. The intensity of this electric dipole transition is stronger than that of Eu^{3+} emission assigned to the $^5D_0 \rightarrow {}^7F_1$ one, observed at around 600 nm, which is assumed as magnetic dipole transition. The bands related to the $^5D_0 \rightarrow {}^7F_3$ transition are observed at around 655 nm. The lifetimes of the Eu^{3+} $^5D_0 \rightarrow {}^7F_0$ transition ($\lambda_{exc.}$ 328 nm and $\lambda_{em.}$ 573 nm) for all the HAP:Eu samples were evaluated from the decay curves, which presented a monoexponential feature. All samples resulted in values of around 0.52 ms, which are in accordance with previously published lifetime for others hydroxyapatite [43].

Conclusions

The milling powder procedure presented as a good approach to obtain pure and Eu^{3+} doped hydroxyapatite. XRD pattern for hydroxyapatites HAPEu0.5, HAPEu1.0, and HAPEu2.0 showed that all samples presented good phase identification when compared to pure hydroxyapatite, indicating that the milling oxide is incorporated, characterizing an interference of the europium in the $Ca_{10}(PO_4)_6O_2$ (HAP) reaction resulted in an excellent substitution of the calcium for the europium ions. Microhardness data for HAP, HAPEu0.5, HAPEu1.0 and HAPEu2.0 samples increase when europium is present in the $Ca_8Eu_2(PO_4)O_2$ (HAP:Eu) structure as Ca^{2+} is replaced by Eu^{3+} during the milling process. This behavior could be related to the morphology of the material since ceramic hardness depends on the grain sizes. It was observed a decrease in the dielectrical constant values as the Eu^{3+} is included in HAP. The incorporation of Eu^{3+} in HAP leads to the formation of the HAP:Eu phase, showing that Eu^{3+} concentration is a very important factor for the dielectrical properties of these materials and is related to the substitution of OH^- for Eu^{3+} ions. The Eu^{3+} doped samples presented a strong and broad excitation band with a maximum at 328 nm, related to the ligand-metal charge transfer into the hydroxyapatite matrix, and a weak band at 391 nm ascribed to the $^5L_6$ level of the Eu^{3+}. The emission spectra of the HAPEu0.5, HAPEu1.0 and HAPEu2.0 samples excited at 328 nm at room temperature shows the $^5D_0 \rightarrow {}^7F_0$ transition at 573 nm, as the main band, where it is noticed a slight shoulder at around 572 nm, indicating the presence of A_1 and A_2 sites. It is well-known that Eu^{3+} substitute Ca^{2+} ions and occupy mainly the Ca (II) sites. The intense $^5D_0$–$^7F_0$ emission band at 573 nm (A_1 and A_2 sites) is related to this substitution, while the weak band at 577 nm (B site) is attributed to substitution on Ca (I). It was not observed a significant change in the spectra feature as the concentration is increased, only a slight difference in its intensity. The decay curves of the Eu^{3+} $^5D_0$–$^7F_0$ transition ($\lambda_{exc.}$ 328 nm and $\lambda_{em.}$ 573 nm) for all HAP:Eu samples presented a monoexponential feature, and all samples resulted in lifetime values of around 0.52 ms.

Acknowledgements The authors wish to thank CAPES, CNPq, FAPESP and Funcap (Brazilian agencies) who partly sponsored this research. We gratefully acknowledge Biomaterials Lab (Metallurgical and Materials Engineering Department, Federal University of Ceará-Brazil) and LOCEM (Physics Department, Federal University of Ceará-Brazil) for the use of their laboratories for sample preparation, and to the Rare earth laboratory of the Chemistry Department of the FFCLRP-USP for luminescence measurements.

References

1. Budin JP, Michel JC, Auzel F (1979) Oscillator-strengths and laser effect in $Na_2Nd_2Pb_6(PO_4)_6Cl_2$ (chloroapatite), a new high-Nd-concentration laser material. J Appl Phys 50:641–646
2. Deloach LD, Payne SA, Smith LK, Kway WL, Krupke WF (1994) Laser and spectroscopic properties of $Sr_5(PO_4)_3F$-Yb. J Opt Soc Am B 11:269–276
3. Wright AO, Seltzer MD, Gruber JB, Chai BHT (1995) Site-selective spectroscopy and determination of energy-levels in Eu^{3+}-doped strontium fluorophosphate. J Appl Phys 78:2456–2467
4. Jagannathan R, Kottaisamy M (1995) Eu^{3+} luminescence—A spectral probe in M(5)(PO_4)(3)X apatites (M=Ca or Sr X=F^-, Cl^-, Br^- or OH^-). J Phys Condens Matter 7:8453–8466
5. Reisfeld R, Gaft M, Boulon G, Panczer C, Jorgensen, CK (1996) Laser-induced luminescence of rare earth elements in natural fluor-apatites. J Lumin 69:343–353
6. Zounani A, Zambon D, Cousseins J (1994) Spectroscopic study of Eu^{3+} in the fluorapatite $Sr_{10}F_2(PO_4)_6$. J Alloys Compd 207:94–98

7. Morozov AM, Morozova LG, Trefimov AK, Feofilov PP (1970) Spectral and luminescent characteristics of fluoropatite single crystals activated by rare earth ions. Opt Spectrosc (USSR) 29:590–598
8. Oweltjes JL (1996) Luminescence and phosphors in modern materials, vol. 5. Academic Press, New York, USA, p 161
9. Lavernia C, Schoenung JM (1991) Calcium-phosphate ceramics as bone substitutes. Am Ceram Soc Bull 70:95–100
10. Sergo V, Sbaizero O, Clarke DR (1997) Mechanical and chemical consequences of the residual stresses in plasma sprayed hydroxyapatite coatings. Biomaterials 18:477–482
11. Yaszemski MJ, Payne RG, Haynes WC, Langer R, Mikos AG (1996) Evolution of bone transplantation: molecular, cellular and tissue strategies to engineer human bone. Biomaterials 17:175–185
12. Liu HS, Chiu TS, Lai SL, Chiu SY, Chung KH, Chang CS, Lui MT (1997) Hydroxyapatite synthesized by a simplified hydrothermal method. Ceram Int 23:19–25
13. Felicio-Fernandes G, Laranjeira MCM (2000) Calcium phosphate biomaterials from marine algae. Hydrothermal synthesis and characterisation. Quim Nova 23:441–446
14. Heimke G (1989) Advanced ceramics for biomedical applications. Angew Chem 101:111–116
15. Hench LL (1991) Bioceramics—From concept to clinic. J Am Ceram Soc 74:1487–1510
16. Bet MR, Gloissis G, Plepis AMD (1997) Collagen: calcium phosphate composites. Preparation and characterization. Quim Nova 20:475–477
17. Toriyama M, Ravaglioli A, Krajewski A, Celotti G, Piancastelli A (1996) Synthesis of hydroxyapatite-based powders by mechanochemical method and their sintering. J Eur Ceram Soc 16:429–436
18. Rhee SH (2002) Synthesis of hydroxyapatite via mechanochemical treatment. Biomaterials 23:1147–1152
19. Silva CC, Pinheiro AG, de Oliveira RS, Goes JC, Aranha N, de Oliveira LR, Sombra ASB (2004). Properties and in vivo investigation of nanocrystalline hydroxyapatite obtained by mechanical alloying. Solid State Sci 6:1365–1374
20. Silva CC, Thomazini D, Pinheiro AG, Lanciotti Jr F, Sasaki JM, Góes JC, Sombra ASB (2002) Optical properties of hydroxyapatite obtained by mechanical alloying. J Phys Chem Solids 63:1745–1757
21. Silva CC, Valente MA, Graça MPF, Sombra ASB (2006) Microwave preparation, structure and electrical properties of calcium–sodium–phosphate biosystem. J Non-Cryst Solids 352:3512–3517
22. Soules TF, Davis TS, Kreidler ER (1971) Molecular orbital model for antimony luminescent centers in fluorophosphate. J Chem Phys 55:1056–1058
23. Budin JP, Neubauer M, Rondot M (1978) Miniature Nd-pentaphosphate laser with bonded mirrors side pumped with low-current-density LEDS. Appl Phys Lett 33:309–311
24. Pappalardo RG, Walsh J, Hunt RB (1983) Cerium-activated halophosphate phosphors. 1. Strontium fluoroapatites. J Electrochem Soc 130:2087–2096
25. Blasse G (1975) Influence of local charge compensation on site occupation and luminescence of apatites. J Solid State Chem 14:181–184
26. Piriou B, Fahmi D, Dexpert-Ghys J, Taitai A, Lacout JL (1987). Unusual fluorescent properties of Eu^{3+} in oxyapatites. J Lumin 39:97–103
27. Voronko YK, Maksimova GV, Sobol AA (1991) Anisotropic centres of TR^{3+}-ion luminescence in fluoroapatite crystals. Opt Spectrosc (USSR) 70:346–351
28. Zounani A, Zambon D, Cousseins JC (1992) Optical-properties of Eu^{3+} activated $Sr_{10}F_2(PO_4)_6$ elaborated by coprecipitation. J Alloys Compd 188:82–86
29. Zounani A, Zambon DJ, Cousseins C (1994) Spectroscopic study of Eu^{3+} in the fluoroapatite $Sr_{10}F_2(PO_4)_6$. J Alloys Compd 207:94–98
30. Wright AO, Seltzer MD, Gruber JB, Chai BHT (1995) Site-selective spectroscopy and determination of energy-levels in Eu^{3+}-doped strontium fluorophosphate. J Appl Phys 78:2456–2467
31. Doat A, Pellé F, Gardant N, Lebugle A (2004) Synthesis of luminescent bioapatite nanoparticles for utilization as a biological probe. J Solid State Chem 177:1179–1187
32. Silva CC (2003) Estudo das Propriedades Ópticas, Elétricas e Térmicas da Hidroxiapatita Obtida por Moagem de Alta energia, seus Compósitos e Filmes Espessos (PhD. Thesis), Fortaleza, Ceará, Brazil
33. JCPDS-Pattern 33-0275 ($Ca_8Eu_2(PO_4)O_2$)
34. Thangamani N, Chinnakali K, Gnanam FD (2002) The effect of powder processing on densification, microstructure and mechanical properties of hydroxyapatite. Ceram Int 28:355–362
35. Lunkenheimer P, Rall P, Alkemper J, Fuess H, Börmer R, Loide A (1995) Ionic motion in bioactive ceramics investigated by dielectric-spectroscopy. Solid State Ion 81:129–134
36. Ozuna O, Hirata G. A, McKittrick (2004). Luminescence enhancement in Eu^{3+}-doped alpha- and gamma-Al_2O_3 produced by pressure-assisted low-temperature combustion synthesis. J Appl Phys Lett 84:1296
37. Sommerdijk JL, Bril A (1976) Position of D-5(0) level of Eu^{3+} in AMGF-3 (A=K, Rb, Cs). J Lumin 12:669–673
38. Rosa ILV, Maciel AP, Longo E, Leite ER, Varela JA (2006) Synthesis and photoluminescence study of $La_{1.8}Eu_{0.2}O_3$ coating on nanometric α-Al_2O_3 Mater Res Bull 41:1791–1797
39. Richardson FS (1982) Terbium(III) and europium(III) ions as luminescent probes and stains for biomolecular systems. Chem Rev 82:541–552
40. Bekiari V, Lianos P (1998) Strongly luminescent poly(ethyleneglycol)-2,2′-bipyridine lanthanide ion complexes. Adv Mater 10:1455–1458
41. Stewart GM, Fox MA (1996) Chromophore-labeled dendrons as light harvesting antennae. J Am Chem Soc 118:4354–4360
42. Ternane R, Trabelsi-Ayedi M, Kbir-Ariguib N, Piriou, B (1999) Luminescent properties of Eu^{3+} in calcium hydroxyapatite. J Lumin 81:165–170
43. Ternane R, Panczer G, Cohen-Adad MT, Goutaudier C, Boulon G, Kbir-Ariguib N, Trabelsi-Ayedi M (2001) Relationships between structural and luminescence properties in Eu^{3+}-doped new calcium borohydroxyapatite. Opt Mater 16:291–300
44. El Ouenzerfi R, Kbir-Ariguib N, Trabelsi-Ayedi M, Piriou B (1999) Spectroscopic study of Eu^{3+} in strontium hydroxyapatite $Sr_{10}(PO_4)_6(OH)_2$. J Lumin 85:71–77